Ultramicroscopy 181 (2017) 61–69

Contents lists available at ScienceDirect

Ultramicroscopy

journal homepage: www.elsevier.com/locate/ultramic

Fast and reliable pre-approach for scanning probe microscopes based on tip-sample capacitance

J.M. de Voogd[a], M.A. van Spronsen[a], F.E. Kalff[b], B. Bryant[b,c], O. Ostojić[a], A.M.J. den Haan[a], I.M.N. Groot[a,d], T.H. Oosterkamp[a], A.F. Otte[b], M.J. Rost[a,*]

[a] Leiden Institute of Physics, Leiden University, P.O. Box 9504, 2300 RA Leiden, The Netherlands
[b] Department of Quantum Nanoscience, Kavli Institute of Nanoscience, Delft University of Technology, Lorentzweg 1, 2628 CJ Delft, The Netherlands
[c] High Field Magnet Laboratory, Radboud University, Toernooiveld 7, 6525 ED Nijmegen, The Netherlands
[d] Leiden Institute of Chemistry, Leiden University, P.O. Box 9502, 2300 RA Leiden, the Netherlands

ARTICLE INFO

Article history:
Received 15 February 2017
Revised 20 April 2017
Accepted 9 May 2017
Available online 10 May 2017

Keywords:
Capacitance measurements
Scanning probe microscope
Scanning tunneling microscope
Nano-positioning
Stepping motor
Coarse approach

ABSTRACT

Within the last three decades Scanning Probe Microscopy has been developed to a powerful tool for measuring surfaces and their properties on an atomic scale such that users can be found nowadays not only in academia but also in industry. This development is still pushed further by researchers, who continuously exploit new possibilities of this technique, as well as companies that focus mainly on the usability. However, although imaging has become significantly easier, the time required for a safe approach (without unwanted tip-sample contact) can be very time consuming, especially if the microscope is not equipped or suited for the observation of the tip-sample distance with an additional optical microscope. Here we show that the measurement of the absolute tip-sample capacitance provides an ideal solution for a fast and reliable pre-approach. The absolute tip-sample capacitance shows a generic behavior as a function of the distance, even though we measured it on several completely different setups. Insight into this behavior is gained via an analytical and computational analysis, from which two additional advantages arise: the capacitance measurement can be applied for observing, analyzing, and fine-tuning of the approach motor, as well as for the determination of the (effective) tip radius. The latter provides important information about the sharpness of the measured tip and can be used not only to characterize new (freshly etched) tips but also for the determination of the degradation after a tip-sample contact/crash.

1. Introduction

Although Scanning Probe Microscopes (SPMs) have clearly demonstrated their power and are used in many different fields [1–25], their usability is still an issue. For example, when comparing to an electron beam technique that can quickly deliver an image of the surface, the user of an SPM has to bring the tip into close vicinity to the sample (pre-approach), thereby avoiding a resolution destroying tip-sample contact (*tip crash*). This requires a careful approach system, which can last even up to ~100 min depending on the microscope, especially if the microscope does not provide optical access. Ideally, one would like to have a fast, robust, and general solution for the approach metrology that can be used in any type of SPM, independently of the design. In this paper we demonstrate a straightforward solution for all SPMs that work with a (semi)conductive tip and sample: the tip-sample distance can accurately be measured via the tip-sample capacitance and this can be used for a quick and robust pre-approach. We also demonstrate that this technique can be applied in tuning-fork based Atomic Force Microscopes (AFMs). Please note that a special class of SPM, the Scanning Capacitance Microscope (SCM), uses the capacitance variation even for imaging and/or spectroscopy [26–29].

For Scanning Tunneling Microscopes (STMs) *with* optical access, the total approach duration is often decreased to acceptable times by using the distance between the tip and its reflection in the sample during a manual pre-approach. In this way the tip-sample distance can be safely decreased to 60 μm, before the user switches to any type of automatic approach.[1]

[1] Usually people work with two different automatic approach routines: (1) with a fully retracted tip, the tip-sample distance is reduced by one (or several) steps of the coarse approach motor, before a feedback checks whether the tip-sample distance is within tunneling range; if this is not the case, the routine will be repeated, (2) with a fully working feedback, the tip-sample distance is reduced continuously, until a tunneling current is detected. Please note that the second method is

* Corresponding author.
E-mail addresses: voogd@physics.leidenuniv.nl (J.M. de Voogd), rost@physics.leidenuniv.nl (M.J. Rost).

http://dx.doi.org/10.1016/j.ultramic.2017.05.009
0304-3991/

However, a fast and reliable manual pre-approach is not always possible, as design aspects of particular SPMs prevent the implementation of optical access (and even cameras). Typical examples are low-temperature STMs, where a closed cryostat, or at least heat shields, are required [30–32]. A solution for these microscopes is the implementation of absolute position readouts, which is often realized by measuring the capacitance between two cylinders that move with respect to each other. However, the position of the tip with respect to the sample remains still unknown, especially after a sample or tip exchange. As a result the (first) approach with a new tip and/or sample usually takes a long time, as one uses the automatic approach right from the beginning to surely prevent a tip-sample contact.

Finally, there are microscopes which can neither implement an optical access nor a capacitive (or any other) readout system [23]. For such systems, a pre-approach based on the tip-sample capacitance, as described in this paper, clearly decreases the total approach time by about a factor of ten.

Faced with the problem that the exact surface position is unknown up to mm after a cleaving process of the sample in a cryogenic dipstick setup, Schlegel et al. [33] found an elegant solution for their pre-approach by measuring the second derivative of the tip-sample capacitance during their approach. Their solution circumvents the determination of the absolute capacitance, which is far from trivial, due to its extremely small value.

In this paper we set the next step and demonstrate that the tip-sample distance can accurately be measured by determining the *absolute* tip-sample capacitance. This enables not only the application of a quick and robust pre-approach, but delivers in addition a tool for an in situ tip-shape and sharpness characterization as well as for measuring and fine-tuning the performance of the coarse-approach motor. Finally, we also demonstrate that this technique can be applied in tuning-fork based Atomic Force Microscopes (AFMs).

We note here that our results combine partially well-established knowledge of different fields: electronics, nanoscale and tip-sample capacitance research, electronic tip-shape modeling, scanning capacitance microscopy, and scanning tunneling microscopy. To comprehensively provide the necessary background information, we review the most important aspects thereby giving credits to the different fields.

In the first section of the paper we present an overview on how to accurately measure absolute capacitances in the femtofarad (fF) and attofarad (aF) regime. We show that there is no need for special electronics. Moreover, it will become clear that, by default, all STMs are optimized for tip-sample capacitance measurements. This insight can be already deduced from Ref. [34] in 2006, in which the authors achieved aF resolution (although not on an absolute scale).

In the second part, we describe measurements on various STMs and one AFM ranging from homebuilt to commercially available systems. To demonstrate the accuracy of this technique, we use a precise automated capacitance bridge. It is remarkable that the same bridge has been used by Kurokawa et al. [35] to study the influence of the tip shape on the tip-sample capacitance already in 1998. However, we also show that less expensive solutions work as well, depending on the specific information one would like to extract (e.g. only the utilization as a pre-approach).

We will show that all measurements have a generic curve, if one plots the capacitance versus the tip-sample distance: it consists of a linear part for large distances and a steep increase for small distances. Similar observations have been obtained before [29,34–37]. However, in addition, we show that the *absolute* capacitance values are in the same order of magnitude (hundreds of fF), although measured with different tips and even on completely different microscopes!

In the last part we elaborate on the generic aspect of the tip-sample capacitance versus distance curve to receive detailed information on the tip geometry. As the tip-sample capacitance determines the resolution in scanning capacitance microscopy, one can find experiments [29,34,35,37,38], analytic descriptions [26,34–39] and finite element models [28,40] in the literature dating back even to 1988 [26]. The growing complexity of the analytical description originates from the desire to explain *all* measured curves with a general equation. However, the tip geometry is not known and has to be assumed. Only Kurokawa et al. [35] measured experimentally their tip shapes with electron microscopy to combine this information further with their model. Building on the earlier work we performed finite element as well as analytical calculations with the practical aim to disentangle the parameters of the geometric tip shape from the measured curves. We show that it is possible to determine the tip radius and sharpness in situ in the microscope, which provides an ideal tool for the user to judge the quality of the tip e.g. after an undesired *tip-crash*. The comparison of our finite element analysis results shows good agreement with the ball model [26] and its later refinement with a dihedral approximation [39]. However, it also becomes clear that the most simple model, the ball model of Kleinknecht et al. [26], fits the data best and is, therefore, in practice the most effective one to use.

2. Subfemtofarad capacitance measurement principles

Using the tip-sample capacitance for the pre-approach requires the capability to measure capacitances with a resolution smaller than one femtofarad. To demonstrate that the capacitance between the tip and the sample delivers an accurate, absolute measure for the tip-sample distance, we measured even with aF resolution. This has been achieved earlier by Fumagalli et al. [34], however, only on a relative scale.

Measuring capacitances within the femtofarad range is not difficult, provided it is performed carefully. There is various commercial electronics available that is suitable for measuring in this capacitance range; usually higher-end electronics allow more accurate and absolute measurements. As most SPMs are not designed for high-frequency applications, we limit ourselves to frequencies below 10 kHz.

It is crucial that the electronic connections leading to the capacitor are separately shielded, as one has to prevent the measurement of so-called *stray capacitances*. For example, two conductors that *see* each other have a stray capacitance which leads to an extra capacitance added to the capacitance of interest. Note that two signal wires close to each other easily have capacitances of hundreds to thousands of femtofarads per *centimeter* [41].

The above explains why it is usually impossible to determine the tip-sample capacitance with a hand-held multimeter: due to stray capacitances, one measures values larger than a picofarad, although one expects (and we will show) that the tip-sample capacitances are in the femtofarad regime. The additional capacitance comes from the signal that goes via the shieldings of the conductors, see Fig. 1a. The proper and ideal solution is to apply an alternating-current (AC) signal to one side of the capacitance, and measure the capacitive current with an amplifier that has a

significantly faster, but often leads to a (not recognized) tip-sample contact when using analog feedback controllers. The reason for this is the integrator in the feedback. This integrator, usually realized as a capacitor, is fully charged to the power supply voltage (here assumed to be positive) during this process. As it integrates the error signal, a reduction of this charge requires a negative voltage of the error signal, which is delivered only if the tip is *closer* to the sample than the *requested* tunneling current set point. This means that, although the tip is already in tunneling conditions, the capacitor is still between zero and full positive voltage, leading to a further approach. Often this electronic circuit is not fast enough to prevent a tip-sample contact.

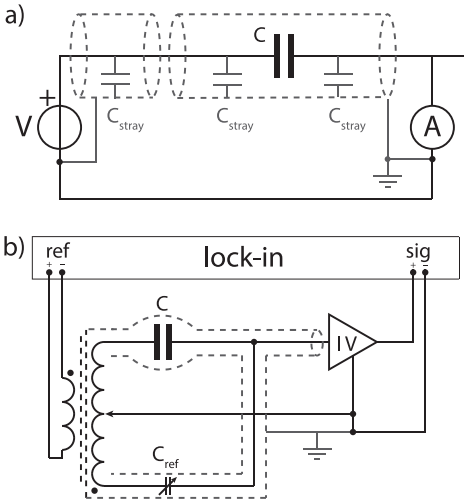

Fig. 1. Working principles of capacitance measurements: a) Schematic of a capacitor with stray capacitances. The low impedance of the current measurement causes the stray capacitances to be negligible. Ideally, the shielding should be connected to ground at one single point in the setup, preferably shortly after the current measurement. b) The resolution and accuracy can be enhanced by using a reference capacitor and a Lock-In. Matching this reference with the unknown capacitor results in a vanishing current, which describes the principles of a capacitance bridge.

low input impedance on the other side of the circuit. A current-to-voltage (IV) converter is the most suited amplifier for this purpose. Please note that a dedicated IV-preamplifier (PreAmp) is inherently installed in every STM. This naturally makes an STM an ideal tool for measuring the tip-sample capacitance. The low input impedance of the PreAmp ensures that the potential difference between the input of the amplifier and the shielding is minimal such that parasitic currents are minimized. The advantage of the PreAmp has also been noticed by Fumagalli et al. [34].

When the signal from the IV-converter is compared to the reference voltage (V_{ref}) by using quadrature measurements (Lock-In), the out-of-phase component (Y) gives a measure for the capacitance:

$$C = \frac{Y}{2\pi f G V_{ref}}. \quad (1)$$

Here, G is the gain of the IV-converter and f the frequency of the reference signal, assuming that the frequency, at which the capacitance measurement is performed, is well below the bandwidth of the IV-converter. This concept for measuring the tip-sample capacitance has been applied by Lee et al. [42], Pingree et al. [43], and Fumagalli et al. [34].

The reproducibility of the above described measurement depends on (possible) changes in the setup, like the (dis)appearance of ground loops. The application of a reference capacitor offers not only a solution for this inaccuracy, it even enables the determination of absolute capacitance measurements. The solution involves the incorporation of the reference capacitor into the electronic measurement circuit in such a way that physical replugging of the cables is not necessary, although the reference capacitor can be turned *on* and *off*. An elegant way is applying the inverted reference voltage over the reference capacitor, before it is added to the signal right in front of the PreAmp, see Fig. 1b. In this way, the reference capacitance is subtracted from the capacitance to be measured. If the reference capacitance exactly matches the capacitance of interest, the output is zero. Even if the capacitance does not match exactly, it is possible to determine the capacitance of interest from the measured (nonzero) signal by precise knowledge of the reference capacitor. Choosing the reference capacitor of the same order of magnitude as the capacitor of interest, makes the output signal smaller and the end result more accurate.

The previous paragraph describes the basic principles of a low-frequency capacitance bridge with high accuracy. Most of the measurements in this paper were performed with an Andeen Hagerlingh capacitance bridge (AH2550) [44], which automatically switches reference capacitances, until the reference value is close to the capacitance of interest. The calibrated reference capacitors are kept at a constant temperature inside an internal oven. This guarantees that the measured capacitance values are of high accuracy and reproducibility. Kurokawa et al. [35] used a similar bridge to accurately characterize the capacitance of their tips, of which they measured the shape before with an electron microscope.

However, as dedicated capacitance bridges can be rather expensive, we will also present results measured with different instruments. The General Radio capacitance bridge [45] requires time consuming, manual switching of the reference capacitors. However, if one only wants to use this bridge for a pre-approach, it is not necessary to zero the signal for each step of the coarse-approach motor. Instead, the reference capacitance is set to a certain, desired threshold value. If the tip-sample capacitance value passes the reference (i.e. the Y-signal on the Lock-In passes zero or the phase rotates 180°), then one knows that the tip enters the range where the automatic approach procedure should be turned on.

Finally, it is easily possible to determine the capacitance directly with dedicated STM electronics, which should be known by researchers that use STMs in spectroscopy mode. If, e.g. the tip is connected to ground via the PreAmp, one can put an AC signal (e.g. 1 V and 10 kHz) on the sample and determine the current through the tip. After the current is converted to a voltage, a Lock-In can be used to determine the out-of-phase component of the signal, from which the capacitance can be calculated using Eq. (1).

However, at all tip-sample distances that are larger than the corresponding tunneling regime, the signal is dominated by the current through the capacitance. Therefore, measuring only the amplitude of the signal is enough to determine the capacitance (and no quadrature measurement, like Lock-In, is needed). For example, just by applying the control electronics described in [46,47], it is possible to measure $\sim$ 10 aF when applying an AC signal of 1 V and 10 kHz to the sample. This concept is applied by Schlegel et al. [33], although they did not work out the absolute capacitances and focused only on the second derivative.

3. Results

To demonstrate the generality of our approach, we investigate various SPMs. We start with an STM that is equipped with an absolute position readout such that one can directly measure the tip-sample capacitance as a function of the distance. After that, we repeat our measurements on systems without position readout and will show that the tip-sample capacitance provides, in addition, an excellent way of determining the coarse-approach motor dynamics and reliability. Furthermore, we will demonstrate the advantage of a fast and safe pre-approach on an STM with a less reliable approach motor and will show that our method works as well for a noncontact AFM [48] that is equipped with a tuning fork.

We start with the JPE-STM: a custom Magnetic Resonance Force Microscopy system (MRFM) that consists of a commercially available stage from JPE [49] with a home-built absolute capacitative position readout. For our purpose, we equipped this stage with an STM tip-holder and a graphite (higly ordered pyrolytic graphite) sample. Applying the AH2550 capacitance bridge, it is possible to measure the absolute position with a precision below 100 nm. Fig. 2 shows the capacitance between tip (including tip holder) and the sample as a function of the tip-sample distance. The curve in Fig. 2 can be used as a calibration of the tip-sample distance by

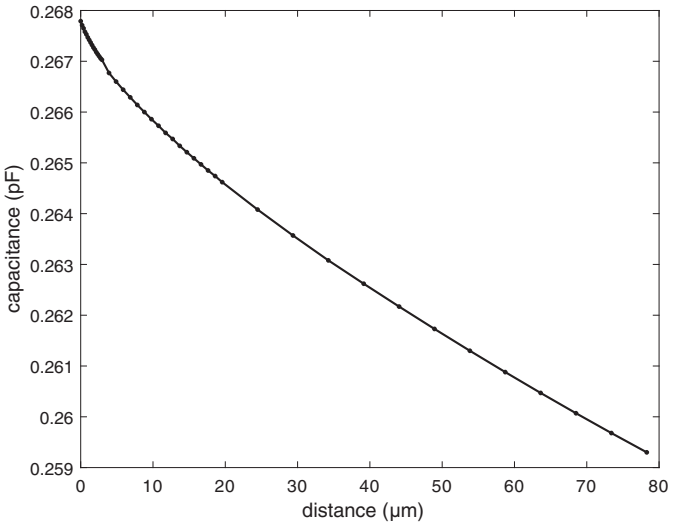

Fig. 2. Tip-sample capacitance measured on the JPE-STM: this microscope is equipped with a homebuilt, capacitive absolute position sensor. Applying a precise capacitance bridge, an independent determination of the tip height is possible. We used a cut PtIr tip and an HOPG sample. The measurement was performed at room temperature and atmospheric pressure.

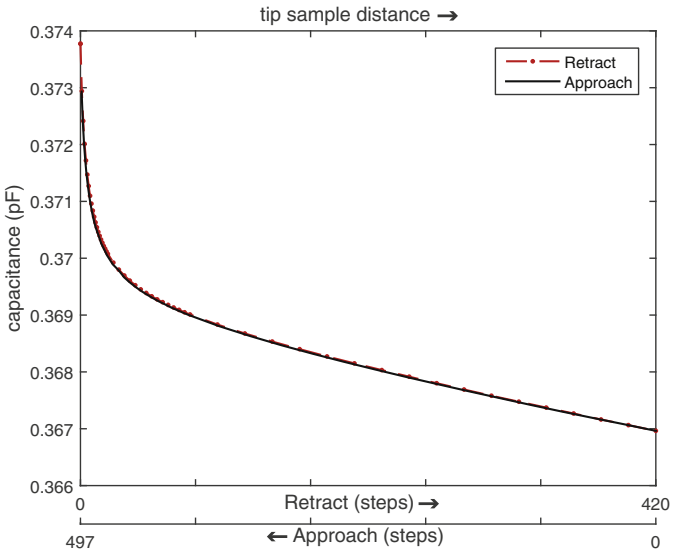

Fig. 3. Tip-sample capacitance measured on a JT-STM: without absolute height, the distance is measured in units of coarse approach motor steps. As the retract curve overlaps exactly with the approach curve (after rescaling), this motor runs reliably over the complete travel range, although the average step size is, due to anisotropic forces, different for both directions. We retracted 420 steps, while we needed 497 steps for the approach. Zero corresponds to a tip-sample distance of 10 nm, which we measured with the calibrated scan piezo. Using this piezo, we also calibrated the step sizes of the motor in the tunneling regime: extrapolating this, 420 retract steps correspond to approximately 10 μm. We used a commercially available PtIr tip and a 120 nm thick Au film on Si as a sample. The temperature during the experiment was 4.6 K.

using the capacitance. This calibration holds even after a sample exchange, provided that the new sample has the same geometry. After a tip change, however, the calibration is usually lost. The influence of the tip with respect to the capacitance-distance curve is explained in detail in Section 4.

As the luxury of an absolute position readout is not present on most SPMs, a calibration like the one shown in Fig. 2 seems to be impossible. This is not fully true, as long as one is not interested in the absolute tip-sample distance in *standard* units. To demonstrate this, we performed a similar measurement on a commercial JT-STM [50], of which the result is shown in Fig. 3. Obviously, one still recognizes a relation between capacitance and distance. However, the distance here is defined in units of coarse-approach motor steps. Please note that, although the retract curve falls exactly on the approach curve, we applied 420 retract steps, but 497 approach ones. Coarse-motor step sizes are usually not very well defined. Therefore, the step size can only be defined as a statistical average. The step size in slip-stick motors can be directionally dependent due to some constant force pushing the slider towards one or the other direction, like gravitational forces or a spring. To account for such an asymmetry, we rescaled the trace for retracting and approaching in Fig. 3 accordingly: it is striking that the curves fall on top of each other quite accurately. This fact together with the smoothness of the curve (and its qualitatively similar shape as in Fig. 2) indicates a reliable motor with linear behavior: the step size is constant over the whole range, although it is different between the approach and retract movement. We determined the step size for retracting and approaching via the calibrated piezo tube, when the system was in tunneling regime. Assuming that these values are representative for the whole measured range, the total distance that the motor traveled was 10 μm.

Unfortunately the average step size of most coarse-approach motors is not only directionally dependent, but varies, in addition, with the precise position of the motor. This is due to imperfections of sliders and surfaces, wear, heavy use at certain positions of the travel range, and other position-dependent effects, like e.g. springs. This becomes clear from an experiment we performed on a heavily used Unisoko-STM [51], of which the results are shown in Fig. 4. To cancel the asymmetry caused by gravity, we applied an analogous directional rescaling as in Fig. 3. Here, however, the retract

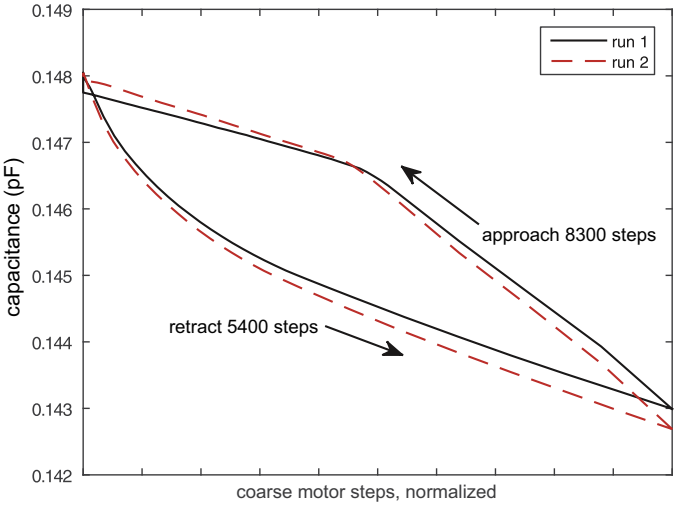

Fig. 4. Tip-sample capacitance measured on a Unisoko-STM: in both runs, we retracted 5490 motor steps and needed 8300 steps to get back. The starting point corresponds to a tip-sample distance of about 10 nm. Note that this motor runs reliably, as both runs fit almost perfectly on top of each other. However, it is obvious that the motor runs with different speeds on different positions of its travel range. Also directional asymmetry is present. We used a commercially available PtIr tip and a Cu(100) sample. These measurements demonstrate that our method can be applied to study the motor performance and dynamics in general. The temperature during the experiment was 1.5 K.

and approach curves do not fall on top of each other. Strikingly, two consecutive experiments (runs) do show reproducibility indicating that the step size does not change significantly in time for a position of the travel range, although there is a huge variation for different positions. As an example, two regions are clearly visible in the approach direction. Our method enables not only the possibility to tune the motor parameters until it moves with constant

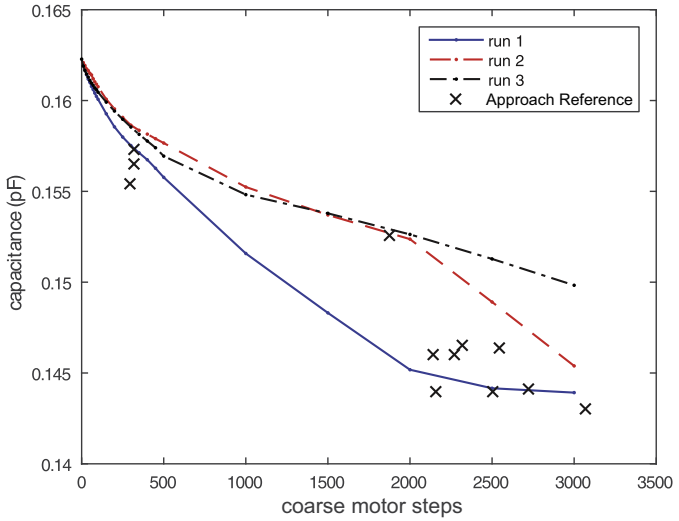

Fig. 5. Tip-sample capacitance measured on the ReactorSTM: the particular design of the approach motor mechanism makes this motor less reliable compared to the approach motors of other STMs. The variation in the motor performance can be seen from three different retract curves. Still it is possible to significantly shorten the total approach time, as is indicated by the crosses, all of which represent an individual approach: based on earlier measured retract curves (run 1–3), the user chooses a *safe* threshold capacitance. The approach motor is continuously operated without extra interrupts until the chosen threshold value is reached. This procedure lasts only a few seconds, after which one switches to the automatic safe (but slower) approach mode and counts the number of steps that are needed to reach the tunneling regime. This procedure lasts only a few tens of seconds. The crosses indicate the chosen threshold capacitance versus the number of steps needed to reach the tunneling regime. To increase the accuracy/statistics, one should measure the capacitance once in a while for a complete retract curve. The data are obtained for different PtIr tips on various (metallic) samples.

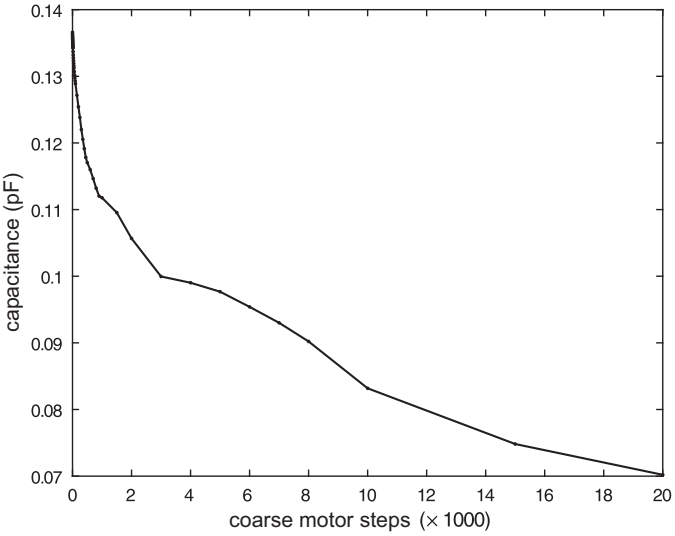

Fig. 6. Tip-sample capacitance measured on the tuning-fork-based AFM: The tuning fork has an electron beam induced deposited tip on one side. This result shows that our quick pre-approach method, which is based on capacitive measurements, is not only applicable to standard STMs.

speed, it even demonstrates the capability to use it for studying coarse-approach motor dynamics in general.

The most rewarding application of the tip-sample capacitance measurement is probably the implementation of it for a fast, safe and reliable pre-approach without optical access. Fig. 5 shows the results for the ReactorSTM [23]. The rather unique coarse-approach mechanism in this STM is realized via a sliding movement of the tip (with tip holder) over two guiding rods at the inside of the scanning piezo tube. Between movements, the tip is magnetically pulled to the guiding rods. Due to this special design, this motor shows nonlinear, and sometimes unpredictable behavior, which is also reflected in the curves of Fig. 5. The combination of this less reliable motor and the absence of optical access, required often long pre-approach times to safely find the tunneling regime.

After a tip exchange, one first measures one (or several) retract curves, which can also be done at ambient conditions if that is more practical. From these curves one can choose a threshold capacitance that one considers to be safe and fast enough (close enough to the sample) for the quick pre-approach. In a next step, one repeatedly runs the approach motor until the threshold value is reached. This happens within a few seconds. Then one switches to the automatic safe (but slower) approach mode and counts the number of steps that are needed to reach the tunneling regime. This procedure lasts only a few tens of seconds. The crosses in Fig. 5 indicate the chosen threshold capacitance versus the number of steps needed to reach the tunneling regime. Applying this way of approaching, the system could be regularly brought into tunneling regime within only 10 minutes, while it took usually 60 minutes and more before. Experience shows that this method is insensitive to sample exchange as long as the samples are of comparable geometry. We expect that a complete approach (including the pre-approach) can be realized in less than a minute, if one programs a dedicated routine for the used control electronics and provided that the motor can move fast enough.

In the final example, we show that the capacitive approach is more widely applicable than to STM only. To illustrate this, we performed a similar measurement using a noncontact AFM equipped with a quartz tuning fork (QTF) [52,61]. Using Electron Beam Induced Deposition (EBID [53]) a nano-sized Pt/C tip was grown on the prong of the tuning fork facing the sample. The length of the tip was $\sim$ 2.6 µm and its diameter was $\sim$ 220 nm. The tip was first approached to the surface by measuring the shift in resonance frequency after every coarse approach step. After the approach, the QTF was retracted in small steps and the capacitance between tip and sample was measured. The results, plotted in Fig. 6, show the same generic curve for the nano-sized tip as observed for the macroscopic STM tips. If one uses a non-conducting tip, one can still use the capacity between the sample and one electrode of the QTF for the pre-approach.

In the above examples we showed *how* the tip-sample capacitance provides valuable information about the tip-sample distance. Even when the capacitance cannot be related to absolute length scales, it still provides information on the motor performance. Depending on the reliability of the motor, the capacitances can be converted into distances in units of motor steps. In any case a reference capacitance can be chosen such that a fast and safe pre-approach can be realized until this value is reached. This method significantly saves time and minimizes the number of tip crash events. In addition, detailed motor characterization and optimization is possible in this way.

4. Finite element analysis

The above presented tip-sample capacitance measurements all show a rather similar curve with a linear behavior for large distances and a steep rise for decreasingly shorter distances. Similar curves have been obtained before [29,34–37]. Moreover, the absolute scale of the values is approximately the same, with the capacitance changing by $5-15$ fF in the last few tens of micrometers. The AFM is an exception to this because the EBID grown tip is very short and the prong of the quartz tuning fork forms a parallel-plate capacitor with the sample surface. Still, the shape of the curve looks similar and suggests a generic behavior which

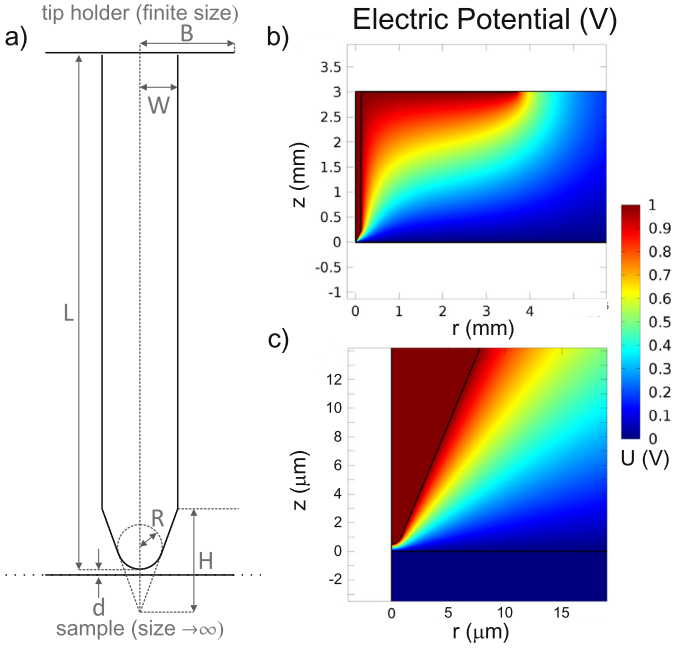

Fig. 7. Simple tip-model a) Schematic of the model (drawn not to scale) of a tip with radius W and length L, connected to a base plate with radius B. The end of the tip is conical with height H and truncated with a ball with radius R. The smallest distance between the tip (the apex) and the relatively large sample is noted d. In our finite element simulations the diameter of the tip wire ($2W$) is fixed to 0.25 mm. To calculate the capacitance in the simulation, we did set the tip to a potential of 1 V and the sample to 0 V. Panels b) and c) show the equipotential lines of the simulation for the particular tip geometry at one distance for the JPE-STM: r denotes the radial direction of the geometry and z is the vertical direction. The simulation was performed with COMSOL [54].

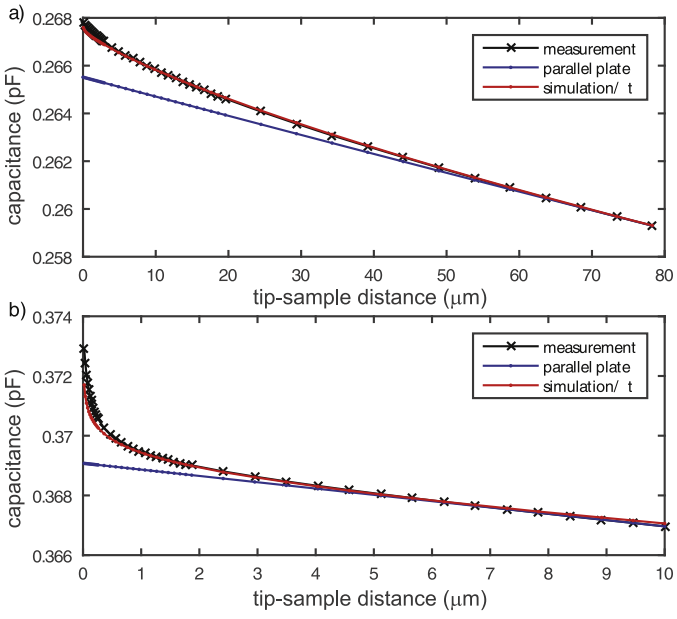

Fig. 8. Comparison between measured, simulated, and analytically calculated data of the tip-sample capacitance. The measurements are shown in black: (a) for the JPE-STM and (b) for the JT-STM. Our simulations (red) closely fit the experimental values. The curve in blue represents an analytical lower boundary based on a parallel-plate approximation.

raises the question: can we also *understand* the tip-sample capacitance curve as function of tip-sample distance?

In order to address this question, we performed a Finite Element Analysis (FEA) [54] calculation and created a simple tip-sample model taking into account cylindrical symmetry, see Fig. 7a. Note that other FEA models have been discussed before [28,40], however, none of them included the tip holder. By simulating the electrical field, shown in Fig. 7b and c, we can determine the capacitance. Finally, by using a parametric sweep for the distance d, which means successive recalculation of the model, we generate a capacitance-distance curve. Furthermore, it is possible to determine the contributions of the tip holder (B), tip length (L), tip sharpness (H), tip wire radius (W), and radius of the apex at the end of the tip (R), as we will describe later in more detail.

To get an estimate for reasonable values of these parameters we can include a lower boundary, which is simply given by a parallel-plate capacitor:

$$C_{par} = \frac{\epsilon_0 A_{par}}{L_{par} + d} \tag{2}$$

C_{par} causes the linear behavior for large tip-sample distances of the total capacitance, see Fig. 8. This additional capacitance comes from the tip holder that forms, in good approximation, with the combination of the sample and sample holder a parallel-plate capacitor. Its capacitance can be easily determined from the data far away from the sample: $A_{par}^{-1} = \epsilon_0 \frac{\partial}{\partial d} C^{-1}\big|_{d_{max}}$ and thus $L_{par} = \epsilon_0 A_{par}/C_{par} - d_{max}$, where d_{max} is the maximum tip-sample distance available in the data. C_{par} is drawn in blue in the graphs of Fig. 8 and the corresponding parameters are provided in Table 1. The remaining deviation for small distances comes from the tip itself and can be described with C_{tip}. Note that L is the real tip length and that L_{par} is the tip length if one assumes the whole capacitance curve could be explained by just one parallel plate at distance $L_{par} + d$. In the following we discuss *how* L as well as the other parameters W, R, H, B influence the capacitance-distance curve. We will show that it is possible to determine all these parameters such that we finally receive fits that closely resemble the measured data, see Fig. 8.

Table 1
This table shows the geometric values that are found by matching the data from Figs. 2 and 3 to the simple model as illustrated in Fig. 7.

	JPE-stage	JT-Specs STM
W	0.126 mm	0.126 mm
L	3.00 mm	3.00 mm
R	1.0 μm	10 μm
H	0.24 mm	0.30 mm
B	3.7 mm	4.7 mm
πB^2	43 mm^2	69 mm^2
A_{par}	98 mm^2	72 mm^2
L_{par}	3.3 mm	1.8 mm

Surprisingly, two branches of analytic descriptions for tip-sample capacitances can be found in literature: the first and older ones [26,35] describe C_{tip} with a sphere, whereas the newer ones consider a cone with a sphere at the end [36,38,39]. In honor of the first description by Kleinknecht et al. [26], we follow this most simplified model to fit and analyze our data. This is fully justified, as we will show in a comparison in Section 5 that the other, more complicated models, do not deliver better fits or insight.

Describing the very end of the tip with a half sphere, the radius of this sphere, R, determines the distance-capacitance curve for small distances ($d < R$). In turn it is possible to derive the radius of the apex from the measured capacitance-distance curves by using [26,35]:

$$R_{eff} = \frac{-1}{2\pi\epsilon_0} \frac{\mathrm{d}C}{\mathrm{d}\ln(d)}, \tag{3}$$

For real small distances ($d \ll R$) R_{eff} converges to the real tip radius R, which we can compare with the R in our simulation that

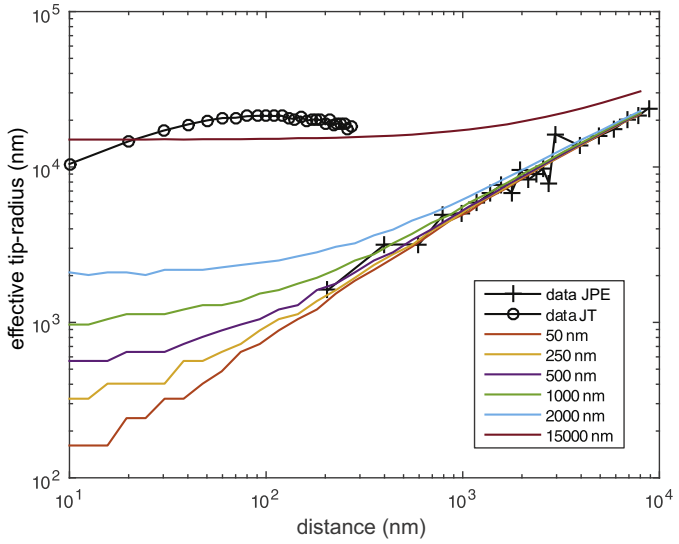

Fig. 9. Effective tip radius, R_{eff}, versus tip-sample distance. Using our simulations, we varied the tip radius R, see Fig. 7, which determines the radius of the apex at the end of the tip. For small tip-sample distances R_{eff} converges to a constant value, which represents the real tip radius. This method provides the possibility to determine the end-of-tip radius (e.g. after a tip crash) *in situ*, in the microscope. For comparison we also plotted the JPE-STM as well as the JT-STM data. Note that the tip in the JT-STM had been crashed before, whereas no tip crash happened in the JPE-STM. This can also be seen from the data of the effective tip radii of the two different microscopes.

fits the measured data. At larger distances C_{par} contributes significantly to the slope of the capacitance-distance curve and therefore R_{eff} is greater than R. This can be seen in Fig. 9, in which we applied Eq. (3) to capacitance-distance FEA data that we calculated for different tip radii R. One sees that when $d \ll R$, R_{eff} indeed converges to the set value R. For completeness, we also plotted the measured data of the JPE-stage (Fig. 2) and the JT-STM (Fig. 3) in Fig. 9. Although clearly different, both data sets fit the theory. The reason for the difference between these two data sets could be tip crashes as well as the different tip fabrication methods (see above).

It becomes clear from this comparison that it is easily possible to determine the apex radius inside the setup, which provides a powerful tool to judge, e.g., if one needs to replace the tip after a tip crash. If one wants to model a measured tip, one should use the lowest measured value for R_{eff}.

Note that it is possible to determine the tip radius (and its sharpness) without the knowledge of the cone height! This finding stands in contrast to previous conclusions [55].

Taking into account the above insight, we fitted the remaining geometric parameters of the tips of the JPE- and the JT-measurements. Table 1 shows the results. From these fits we learned about their dependencies:

In the 1–100 µm micron tip-sample distance regime, L and B contribute in the same manner: they act mainly as an offset to the capacitance curve. As the total tip length can be rather accurately determined and is usually even similar for different microscopes, the main difference often comes from C_{par}, which is due to the specific tip-holder design (described by B). For the fit in Fig. 8 we did set L to a fixed, realistic value of 3 mm and varied B as a fitting parameter. The second fitting parameter is given by the cone height H that describes the macroscopic sharpness at the tip end. In the large-distance regime (1 to 100 micron), this sharpness determines mainly the general slope of the curve, such that this parameter can be determined independently. The last missing parameter is W, which is set by the used tip wire; 126 µm in our case. In conclusion, to receive the fits presented in Fig. 8, we determined first the real tip radius R (see Fig. 9) and further needed only an optimization of the geometric parameters B and H that determine the offset and slope, respectively, for the large distance range.

As a remark, please note that the values in Tab. 1 are not exactly representative for the geometry of the real tips and tip-holders, especially as the geometry of real tip holders can be complicated. However, it is striking that this simple model generates two different curves that follow the capacitance-distance curves of two completely different measured systems remarkably well, see Fig. 9.

Despite this fact, a careful comparison between the simulated curve (red) and the measured data (black) in Fig. 8 reveals too low capacitances of the fit for small distances. Speculating on the reason, we suspect that the extra capacitance in the experimental data stems from the roughness (imperfections) of the surface of the sphere, like protrusions, that are not included in the model. The additional charge buildup by these protrusions is expected to be commonly found for cut PtIr tips due to the tendency of this material to form micro-tips under cutting. How the capacitance is influenced by the surface roughness can be calculated [56–58]. However, the reverse, how to calculate the roughness of the STM tip based on the additional capacitances in the capacitance-distance curve, remains an interesting open question that is beyond the scope of this paper.

5. Analytical models

For the purpose of scanning capacitance microscopy, various analytical formulas have been developed that describe the (slope of the) capacitance as a function of tip-sample distance [26,34–39]. One of the earliest contributions [26,35] state that the variation of the capacitance, $\partial C/\partial d$, comes mainly from the ball-shaped apex (with radius R) in the regime where $d \ll R$. For a ball approaching an infinite plane, this variation is given by [26]:

$$\frac{\partial C_{tip}}{\partial d} \approx -2\pi\epsilon_0 \frac{R}{d} \tag{4}$$

Realizing that a real tip does consist of a combination of a ball with a cone, a refined formula was derived a decade later by using a dihedral approximation [39]. The result,

$$\frac{\partial C_{tip}}{\partial d} \approx -2\pi\epsilon_0 \left[\frac{R}{d} \frac{1}{1+\frac{d}{R(1-\sin\theta)}} + \frac{1}{\ln^2 \tan(\theta/2)} \times \left(\ln \frac{d+R(1-\sin\theta)}{H+R(1-\cot\theta)} - 1 + \frac{1+\frac{1}{\sin\theta}}{1+\frac{d}{R(1-\sin\theta)}} \right) \right], \tag{5}$$

is less straightforward since it also involves the cone of the tip that is described by its angle θ, i.e. $\tan\theta = W/H$, see Fig. 7. Please note that only the first term in the square brackets comes from the ball-shaped end of the tip. Moreover, following the derivation in Ref. [39] one realizes that Eq. (4) was used as a boundary condition for deriving the first term in Eq. (5). Since this term dominates at small distances, it is not at all surprising that Eq. (5) breaks down to Eq. (4) in this regime ($d \ll R$). Noticing that the tip radius influences the total capacitance only for small distances, at which the radius can be determined experimentally, the added value of Eq. (5) should be the description of the total capacitance for rather large distances ($d \geq R$). Equipped with the complete FEA tip model, in which we easily can change the tip radii, we tested both analytical descriptions against the FEA model.

Fig. 10 shows the result, in which the solid colored lines are for different radii obtained from the FEA calculations. Our results nicely match those published by Lányi et al. [55], who calculated the variation of the tip-sample capacitance for a tip with R = 100 nm. To evaluate the analytic theories, we fitted (dashed

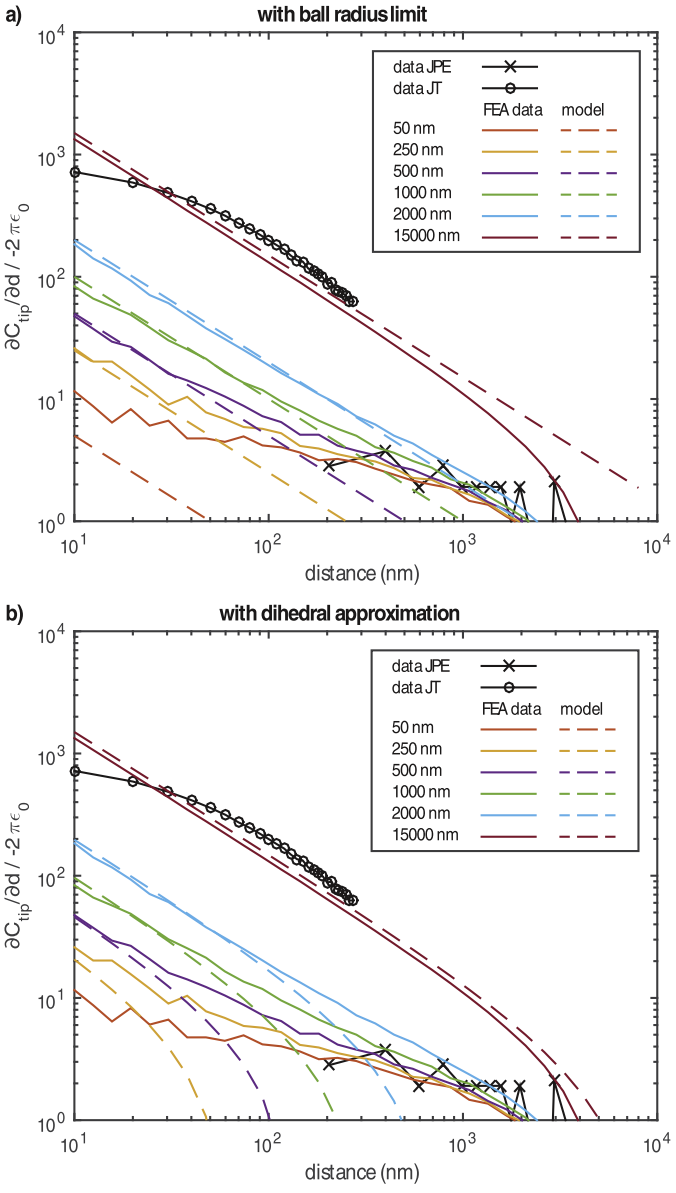

Fig. 10. Comparison of two analytical models: (a) the ball model described by Eq. (4), and (b) the dihedral model described by Eq. (5). The dashed lines represent the models, whereas the solid lines show the FEA results. Everything is calculated for different tip radii that are represented by different colors. For completeness we also added the JPE and JT data in black.

lines) our results with the ball model (Eq. (4)) in Fig. 10a, and with the dihedral approximation model (Eq. (5)) in Fig. 10b. Comparing the fits one realizes three important points: (1) As expected, there is little difference for small distances (compare offset values at the y-axis); (2) The ball model describes straight lines, whereas the dihedral-approximation model curves "down" to lower values at a distance $d \sim \frac{1}{10}R$. (3) In contradiction, the FEA results curve "up" for large distances.

From this we can conclude that the dihedral-approximation model is not suited to describe the large-distance behavior [59]. The reason for this is that the cone ends at a certain height (see Fig. 7a) and that the tip should be described from this point on with a straight wire that ends in a plate of a capacitor (shield).

This means that fitting the cone angle directly from Eq. (5) is unreliable. As the ball radius is equally well derived from Eq. (4), there is no advantage to continue using Eq. (5). Therefore we used Eq. (4) to determine the radius of the ball-shaped apex, see Section 4. Currently, if one needs to determine the cone angle, one should still create a realistic FEA model.

6. Conclusion

We showed that it is possible to determine the absolute distance between a tip and a sample via the capacitance between them. Although the capacitances are in the order of tenths to hundreds of femtofarads, the tip-sample separations can be measured reliably for both large scale as well as nanometer distances. Measuring such low capacitances with high accuracy seems to be a difficult task. However, we showed that the application of a low input impedance current-to-voltage converter in combination with proper grounding and shielding makes this task rather easy, as stray capacitances are eliminated in this way. Moreover, by applying an STM control electronics it is possible to measure $\sim$ 10 aF (and even below). We measured the tip-sample capacitance versus distance on several different setups with different tips and samples and found a generic curve with even similar absolute values. Our analysis provides deeper insight and delivers additional benefit for the user, as it is possible to extract the tip shape and radius from these curves. We find, in contrast to earlier conclusions, that it is possible to determine the tip radius without the knowledge of the height of the conical part of the tip. This is a powerful tool to determine the actual quality of a tip, whether it is freshly etched or has experienced a tip crash. We compared our FEA results with analytic theories and found that the most simple model, the ball model approximation [26], delivers the best fit and should, therefore, be used in most cases. Probably the most important impact, however, is the implementation of a fast and reliable pre-approach for any type of SPM and especially for those that do not provide optical access, thereby significantly reducing the total approach time before imaging. Furthermore, it is possible to use the tip-sample capacitance as a characterization tool of the motor performance of the SPM: motor fine tuning, deterioration, and problem analysis can be performed in this way. Finally, the determination of the absolute tip-sample capacitance (including the tip holder) is crucial for a proper system characterization when working in the GHz regime [31]. The capacitance determines, in addition, the energy broadening of an STM when reaching the quantum limit at ultra-low temperatures [60].

References

[1] D.M. Eigler, E.K. Schweizer, Positioning single atoms with a scanning tunnelling microscope, Nature 344 (6266) (1990) 524–526, doi:10.1038/344524a0.
[2] A boy and his atom: the world's smallest movie, 2013, http://www.research.ibm.com/articles/madewithatoms.shtml .
[3] M.F. Crommie, C.P. Lutz, D.M. Eigler, Confinement of electrons to quantum corrals on a metal surface, Science 262 (5131) (1993) 218–220, doi:10.1126/science.262.5131.218.
[4] P. Liljeroth, J. Repp, G. Meyer, Current-induced hydrogen tautomerization and conductance switching of naphthalocyanine molecules, Science 317 (5842) (2007) 1203–1206, doi:10.1126/science.1144366.
[5] R. Wiesendanger, I.V. Shvets, D. Bürgler, G. Tarrach, H.J. Güntherodt, J.M.D. Coey, Recent advances in spin-polarized scanning tunneling microscopy, Ultramicroscopy 42 (1992) 338–344, doi:10.1016/0304-3991(92)90289-V.
[6] A.A. Khajetoorians, A.J. Heinrich, Toward single-atom memory, Science 352 (6283) (2016) 296–297, doi:10.1126/science.aaf2481.
[7] P. Vettiger, M. Despont, U. Drechsler, U. Durig, W. Haberle, M.I. Lutwyche, H.E. Rothuizen, R. Stutz, R. Widmer, G.K. Binnig, The "Millipede";- More than thousand tips for future AFM storage, IBM J. Res. Dev. 44 (3) (2000) 323–340, doi:10.1147/rd.443.0323.
[8] A.J. Heinrich, C.P. Lutz, J.A. Gupta, D.M. Eigler, Molecule cascades, Science 298 (5597) (2002) 1381–1387, doi:10.1126/science.1076768.
[9] A.A. Khajetoorians, J. Wiebe, B. Chilian, R. Wiesendanger, Realizing all-spinbased logic operations atom by atom, Science 332 (6033) (2011) 1062–1064, doi:10.1126/science.1201725.
[10] P. Roushan, J. Seo, C.V. Parker, Y.S. Hor, D. Hsieh, D. Qian, A. Richardella, M.Z. Hasan, R.J. Cava, A. Yazdani, Topological surface states protected from backscattering by chiral spin texture, Nature 460 (7259) (2009) 1106–1109, doi:10.1038/nature08308.

[11] E. Matsuyama, T. Kondo, H. Oigawa, D. Guo, S. Nemoto, J. Nakamura, Principles and application of heterodyne scanning tunnelling spectroscopy, Sci. Rep. 4 (2014) 6711, doi:10.1038/srep06711.

[12] D. Hoffmann, J. Seifritz, B. Weyers, R. Möller, Thermovoltage in scanning tunneling microscopy, J. Electr. Spectrosc. Relat. Phenom. 109 (12) (2000) 117–125, doi:10.1016/S0368-2048(00)00111-0.

[13] R. Merry, M. Uyanik, R. van de Molengraft, R. Koops, M. van Veghel, M. Steinbuch, Identification, control and hysteresis compensation of a 3 DOF metrological AFM, Asian J. Control 11 (2) (2009) 130–143, doi:10.1002/asjc.89.

[14] D.G. Yablon, Overview of atomic force microscopy, in: D.G. Yablon (Ed.), Scanning probe microscopy in industrial applications, John Wiley & Sons, Inc, 2013, pp. 1–14.

[15] H. Sadeghian, R. Herfst, J. Winters, W. Crowcombe, G. Kramer, T.v.d. Dool, M.H.v. Es, Development of a detachable high speed miniature scanning probe microscope for large area substrates inspection, Rev. Sci. Instrum. 86 (11) (2015) 113706, doi:10.1063/1.4936270.

[16] G.E. Engelmann, J.C. Ziegler, D.M. Kolb, Electrochemical fabrication of large arrays of metal nanoclusters, Surf. Sci. 401 (2) (1998) L420–L424, doi:10.1016/S0039-6028(98)00078-8.

[17] L. Gross, F. Mohn, N. Moll, P. Liljeroth, G. Meyer, The chemical structure of a molecule resolved by atomic force microscopy, Science 325 (5944) (2009) 1110–1114, doi:10.1126/science.1176210.

[18] F.J. Giessibl, S. Hembacher, H. Bielefeldt, J. Mannhart, Subatomic features on the Silicon (111)-(7x7) surface observed by atomic force microscopy, Science 289 (5478) (2000) 422–425, doi:10.1126/science.289.5478.422.

[19] Y. Sugimoto, Atomic force microscopy for imaging, identification and manipulation of single atoms, e-J. Surf. Sci. Nanotechnol. 14 (2016) 28–34, doi:10.1380/ejssnt.2016.28.

[20] M.J. Rost, In situ real-time observation of thin film deposition: roughening, zeno effect, grain boundary crossing barrier, and steering, Phys. Rev. Lett. 99 (26) (2007) 266101, doi:10.1103/PhysRevLett.99.266101.

[21] P.K. Hansma, J.P. Cleveland, M. Radmacher, D.A. Walters, P.E. Hillner, M. Bezanilla, M. Fritz, D. Vie, H.G. Hansma, C.B. Prater, J. Massie, L. Fukunaga, J. Gurley, V. Elings, Tapping mode atomic force microscopy in liquids, Appl. Phys. Lett. 64 (13) (1994) 1738–1740, doi:10.1063/1.111795.

[22] T. Ando, N. Kodera, E. Takai, D. Maruyama, K. Saito, A. Toda, A high-speed atomic force microscope for studying biological macromolecules, Proc. Nat. Acad. Sci. 98 (22) (2001) 12468–12472, doi:10.1073/pnas.211400898.

[23] C.T. Herbschleb, P.C.v.d. Tuijn, S.B. Roobol, V. Navarro, J.W. Bakker, Q. Liu, D. Stoltz, M.E. Cañas-Ventura, G. Verdoes, M.A.v. Spronsen, M. Bergman, L. Crama, I. Taminiau, A. Ofitserov, G.J.C.v. Baarle, J.W.M. Frenken, The ReactorSTM: atomically resolved scanning tunneling microscopy under high-pressure, high-temperature catalytic reaction conditions, Rev. Sci. Instruments 85 (8) (2014) 083703, doi:10.1063/1.4891811.

[24] Y.I. Yanson, M.J. Rost, Structural accelerating effect of chloride on copper electrodeposition, Angewandte Chemie Int. Edi. 52 (9) (2013) 2454–2458, doi:10.1002/anie.201207342.

[25] R. Garcia, E.T. Herruzo, The emergence of multifrequency force microscopy, Nature Nanotechnol. 7 (4) (2012) 217–226, doi:10.1038/nnano.2012.38.

[26] H.P. Kleinknecht, J.R. Sandercock, H. Meier, An experimental scanning capacitance microscope, Scanning Microsc. 2 (4) (1988) 1839–1844.

[27] Š. Lányi, M. Hruškovic, Analysis of lateral resolution and contrast of scanning capacitance microscopes, Surf. Sci. 566568, Part 2 (2004) 880–884. Proceedings of the 22nd European Conference on Surface Science. http://dx.doi.org/10.1016/j.susc.2004.06.025.

[28] D.T. Lee, J.P. Pelz, B. Bhushan, Scanning capacitance microscopy for thin film measurements, Nanotechnology 17 (5) (2006) 1484, doi:10.1088/0957-4484/17/5/054.

[29] L. Fumagalli, G. Ferrari, M. Sampietro, G. Gomila, Dielectric-constant measurement of thin insulating films at low frequency by nanoscale capacitance microscopy, Appl. Phys. Lett. 91 (24) (2007) 243110, doi:10.1063/1.2821119.

[30] Y.J. Song, A.F. Otte, V. Shvarts, Z. Zhao, Y. Kuk, S.R. Blankenship, A. Band, F.M. Hess, J.A. Stroscio, Invited review article: a 10 mK scanning probe microscopy facility, Rev. Sci. Instruments 81 (12) (2010) 121101, doi:10.1063/1.3520482.

[31] B. Jäck, M. Eltschka, M. Assig, A. Hardock, M. Etzkorn, C.R. Ast, K. Kern, A nanoscale gigahertz source realized with Josephson scanning tunneling microscopy, Appl. Phys. Lett. 106 (1) (2015) 013109, doi:10.1063/1.4905322.

[32] F. Donati, S. Rusponi, S. Stepanow, C. Wckerlin, A. Singha, L. Persichetti, R. Baltic, K. Diller, F. Patthey, E. Fernandes, J. Dreiser, Ž. Šljivančanin, K. Kummer, C. Nistor, P. Gambardella, H. Brune, Magnetic remanence in single atoms, Science 352 (6283) (2016) 318–321, doi:10.1126/science.aad9898.

[33] R. Schlegel, T. Hnke, D. Baumann, M. Kaiser, P.K. Nag, R. Voigtlnder, D. Lindackers, B. Bchner, C. Hess, Design and properties of a cryogenic dip-stick scanning tunneling microscope with capacitive coarse approach control, Rev. Sci. Instruments 85 (1) (2014) 013706, doi:10.1063/1.4862817.

[34] L. Fumagalli, G. Ferrari, M. Sampietro, I. Casuso, E. MartÃnez, J. Samitier, G. Gomila, Nanoscale capacitance imaging with attofarad resolution using ac current sensing atomic force microscopy, Nanotechnology 17 (18) (2006) 4581–4587, doi:10.1088/0957-4484/17/18/009.

[35] S. Kurokawa, A. Sakai, Gap dependence of the tip-sample capacitance, J. Appl. Phys. 83 (12) (1998) 7416–7423, doi:10.1063/1.367985.

[36] G. Gomila, J. Toset, L. Fumagalli, Nanoscale capacitance microscopy of thin dielectric films, J. Appl. Phys. 104 (2) (2008) 024315, doi:10.1063/1.2957069.

[37] G. Gomila, G. Gramse, L. Fumagalli, Finite-size effects and analytical modeling of electrostatic force microscopy applied to dielectric films, Nanotechnology 25 (25) (2014) 255702, doi:10.1088/0957-4484/25/25/255702.

[38] B.M. Law, F. Rieutord, Electrostatic forces in atomic force microscopy, Phys. Rev. B 66 (3) (2002) 035402, doi:10.1103/PhysRevB.66.035402.

[39] S. Hudlet, M.S. Jean, C. Guthmann, J. Berger, Evaluation of the capacitive force between an atomic force microscopy tip and a metallic surface, Eur. Phys. J. B - Cond. Matter Complex Syst. 2 (1) (1998) 5–10, doi:10.1007/s100510050219.

[40] S. Lnyi, M. Hruskovic, The resolution limit of scanning capacitance microscopes, J. Phys. D 36 (5) (2003) 598, doi:10.1088/0022-3727/36/5/326.

[41] For example: RG58 coaxial cable has 82 pF/m.

[42] D.T. Lee, J.P. Pelz, B. Bhushan, Instrumentation for direct, low frequency scanning capacitance microscopy, and analysis of position dependent stray capacitance, Rev. Sci. Instruments 73 (10) (2002) 3525–3533, doi:10.1063/1.1505655.

[43] L.S.C. Pingree, E.F. Martin, K.R. Shull, M.C. Hersam, Nanoscale impedance microscopy-a characterization tool for nanoelectronic devices and circuits, IEEE Trans. Nanotechnol. 4 (2) (2005) 255–259, doi:10.1109/TNANO.2004.837856.

[44] AH2550 ultra-precision capacitance bridge, Andeen-Hagerlingh (2014).

[45] GenRad 1615-A, general radio company (~1970).

[46] M.J. Rost, G.J.C. van Baarle, A.J. Katan, W.M. van Spengen, P. Schakel, W.A. van Loo, T.H. Oosterkamp, J.W.M. Frenken, Video-rate scanning probe control challenges: setting the stage for a microscopy revolution, Asian J. Control 11 (2) (2009) 110–129, doi:10.1002/asjc.88.

[47] M.J. Rost, L. Crama, P. Schakel, E.v. Tol, G.B.E.M.v. Velzen-Williams, C.F. Overgauw, H.t. Horst, H. Dekker, B. Okhuijsen, M. Seynen, A. Vijftigschild, P. Han, A.J. Katan, K. Schoots, R. Schumm, W.v. Loo, T.H. Oosterkamp, J.W.M. Frenken, Scanning probe microscopes go video rate and beyond, Rev. Sci. Instruments 76 (5) (2005) 053710, doi:10.1063/1.1915288.

[48] S.B. Roobol, M.E. Cañas-Ventura, M. Bergman, M.A.v. Spronsen, W.G. Onderwaater, P.C.v.d. Tuijn, R. Koehler, A. Ofitserov, G.J.C.v. Baarle, J.W.M. Frenken, The ReactorAFM: non-contact atomic force microscope operating under high-pressure and high-temperature catalytic conditions, Rev. Sci. Instruments 86 (3) (2015) 033706, doi:10.1063/1.4916194.

[49] High resonance cryo positioning stage, Janssen precision engineering (2014). URL http://janssenprecisionengineering.com.

[50] Joule–Thomson low-temperature scanning probe microscope with tyto head, SPECS (2014). URL http://specs.de.

[51] USM1300S-3He, Unisoko (2011). URL http://www.unisoku.com/.

[52] Similar to the qPlus sensor of Giessibl et al., [61].

[53] Nova NanoSEM 200, FEI.

[54] COMSOL Multiphysics®v. 5.2. COMSOL AB, Stockholm, Sweden (2015). URL http://comsol.com.

[55] Š. Lányi, Effect of tip shape on capacitance determination accuracy in scanning capacitance microscopy, Ultramicroscopy 103 (3) (2005) 221–228. http://dx.doi.org/10.1016/j.ultramic.2004.12.002.

[56] L. Boyer, F. Houze, A. Tonck, J.-L. Loubet, J.-M. Georges, The influence of surface roughness on the capacitance between a sphere and a plane, J. Phys. D 27 (7) (1994) 1504, doi:10.1088/0022-3727/27/7/024.

[57] N.C. Bruce, A. García-Valenzuela, D. Kouznetsov, Rough-surface capacitor: approximations of the capacitance with elementary functions, J. Phys. D 32 (20) (1999) 2692, doi:10.1088/0022-3727/32/20/317.

[58] N.C. Bruce, A. García-Valenzuela, D. Kouznetsov, The lateral resolution limit for imaging periodic conducting surfaces in capacitive microscopy, J. Phys. D 33 (22) (2000) 2890, doi:10.1088/0022-3727/33/22/305.

[59] It was found by experiments [38] that sometimes the model would better be replaced by a hyperboloid model. However, in our FEA simulations we fixed the geometry to be ball-shaped+cone and not hyperboloid.

[60] C.R. Ast, B. Jck, J. Senkpiel, M. Eltschka, M. Etzkorn, J. Ankerhold, K. Kern, Sensing the quantum limit in scanning tunnelling spectroscopy, Nat. Commun. 7 (2016) 13009, doi:10.1038/ncomms13009.

[61] F.J. Giessibl, S. Hembacher, M. Herz, C. Schiller, J. Mannhart, Stability considerations and implementation of cantilevers allowing dynamic force microscopy with optimal resolution: the qPlus sensor, Nanotechnology 15 (2) (2004) S79.